Figure S1

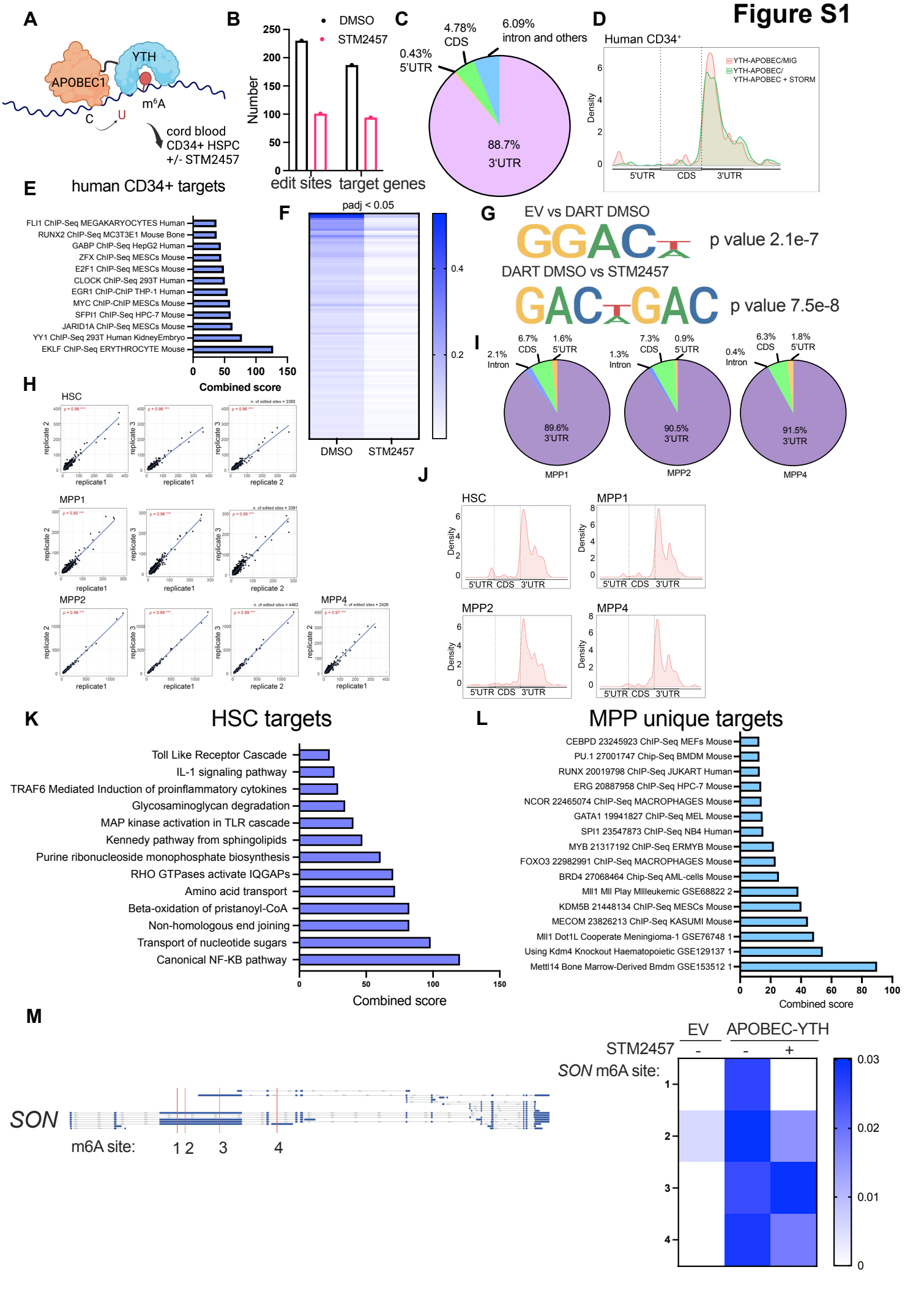
A
APOBEC1
YTH
m6A
C
U
cord blood
CD34+ HSPC
+/- STM2457
B
DMSO
STM2457
Number
edit sites
target genes
C
4.78%
CDS
6.09%
intron and others
0.43%
5'UTR
88.7%
3'UTR
D
Human CD34+
YTH-APOBEC/MIG
YTH-APOBEC/
YTH-APOBEC + STORM
Density
5'UTR
CDS
3'UTR
E
human CD34+ targets
FLI1 ChIP-Seq MEGAKARYOCYTES Human
RUNX2 ChIP-Seq MC3T3E1 Mouse Bone
GABP ChIP-Seq HepG2 Human
ZFX ChIP-Seq MESCs Mouse
E2F1 ChIP-Seq MESCs Mouse
CLOCK ChIP-Seq 293T Human
EGR1 ChIP-ChIP THP-1 Human
MYC ChIP-ChIP MESCs Mouse
SFPI1 ChIP-Seq HPC-7 Mouse
JARID1A ChIP-Seq MESCs Mouse
YY1 ChIP-Seq 293T Human KidneyEmbryo
EKLF ChIP-Seq ERYTHROCYTE Mouse
Combined score
F
padj < 0.05
DMSO
STM2457
G
EV vs DART DMSO
p value 2.1e-7
DART DMSO vs STM2457
p value 7.5e-8
H
HSC
MPP1
MPP2
MPP4
replicate 1
replicate 2
replicate 3
I
2.1%
Intron
6.7%
CDS
1.6%
5'UTR
89.6%
3'UTR
MPP1
1.3%
Intron
7.3%
CDS
0.9%
5'UTR
90.5%
3'UTR
MPP2
0.4%
Intron
6.3%
CDS
1.8%
5'UTR
91.5%
3'UTR
MPP4
J
HSC
MPP1
MPP2
MPP4
Density
5'UTR CDS 3'UTR
K
HSC targets
Toll Like Receptor Cascade
IL-1 signaling pathway
TRAF6 Mediated Induction of proinflammatory cytokines
Glycosaminoglycan degradation
MAP kinase activation in TLR cascade
Kennedy pathway from sphingolipids
Purine ribonucleoside monophosphate biosynthesis
RHO GTPases activate IQGAPs
Amino acid transport
Beta-oxidation of pristanoyl-CoA
Non-homologous end joining
Transport of nucleotide sugars
Canonical NF-KB pathway
Combined score
L
MPP unique targets
CEBPD 23245923 ChIP-Seq MEFs Mouse
PU.1 27001747 Chip-Seq BMDM Mouse
RUNX 20019798 ChIP-Seq JUKART Human
ERG 20887958 ChIP-Seq HPC-7 Mouse
NCOR 22465074 ChIP-Seq MACROPHAGES Mouse
GATA1 19941827 ChIP-Seq MEL Mouse
SPI1 23547873 ChIP-Seq NB4 Human
MYB 21317192 ChIP-Seq ERMYB Mouse
FOXO3 22982991 ChIP-Seq MACROPHAGES Mouse
BRD4 27068464 Chip-Seq AML-cells Mouse
MII1 MII Play MIIleukemic GSE68822 2
KDM5B 21448134 ChIP-Seq MESCs Mouse
MECOM 23826213 ChIP-Seq KASUMI Mouse
MII1 Dot1L Cooperate Meningioma-1 GSE76748 1
Using Kdm4 Knockout Haematopoietic GSE129137 1
Mettl14 Bone Marrow-Derived Bmdm GSE153512 1
Combined score
M
SON
m6A site:
1 2
3
4
EV
APOBEC-YTH
STM2457
-
-
+
SON m6A site:
1
2
3
4

Supplementary Figure 1: DART-seq identifies SON as a conserved m^{6}A target in mouse and human HSCs. Related to Figure 1.

(A) Schematic illustration of the DART-seq experiment in purified human CD34+ cells treated with or without the METTL3 inhibitor STM2457 (20μM for 2 days).
(B) DART-seq identified significant editing sites and gene targets in purified human CD34+ cells treated with or without the METTL3 inhibitor STM2457. n=3, three independent experiments. Edit sites and gene targets were compared between CD34+ APOBEC-YTH DMSO vs empty vector; or CD34+ APOBEC-YTH STM2457 vs empty vector samples. Sites with adjusted p.binomial<0.05 were defined as significant.
(C) DART-seq gene targets in purified human CD34+ cells were mainly localized to 3'UTR.
(D) Metagene plot of DART-seq in human CD34+ cells treated with or without the METTL3 inhibitor STM2457 target sites showed an enrichment of editing close to the stop codon.
(E) Enrichr pathway analysis using the human CD34+ cells DART-seq targets.
(F) METTL3 inhibitor STM2457 treatment significantly reduced the editing frequency on the DART-seq targets in purified human CD34+ cells. Sites were compared between CD34+ APOBEC-YTH DMSO sample and CD34+ APOBEC-YTH STM2457 sample. Sites with adjusted p.binomial<0.05 were defined as significant, n=3 independent experiments.
(G) m6A DRACH motif is enriched in DART-seq sites. Sites with a log2Fold edit greater than 1.5 and adjusted P value < 0.05 were defined as significantly edited sites.
(H) Reproducibility of the DART-seq data. Correlation of the total edited reads per site across the replicates containing the YTH-APOBEC construct (Pearson correlation in red, P value < 0.001 and indicated by ***).
(I) DART-seq targets in mouse MPP populations were mainly localized to 3'UTR.
(J) Metagene plot of DART-seq target sites in mouse HSC and MPPs showed an enrichment of editing close to the stop codon.
(K) Enrichr pathway analysis using the mouse HSC DART-seq targets.
(L) Enrichr pathway analysis using the mouse MPP DART-seq targets that are not shared with HSCs.
(M) Three out of four m^{6}A sites on the SON transcript are sensitive to STM2457 treatment. Location of m^{6}A sites on the *SON* transcript in human CD34+ cells were shown. Red vertical lines indicate the location of each m^{6}A sites (Site 1,2,3,4). Heatmap of C to U editing frequency of each site in EV (empty vector) or APOBEC-YTH overexpressing CD34+ cells treated with or without STM2457.

Figure S2

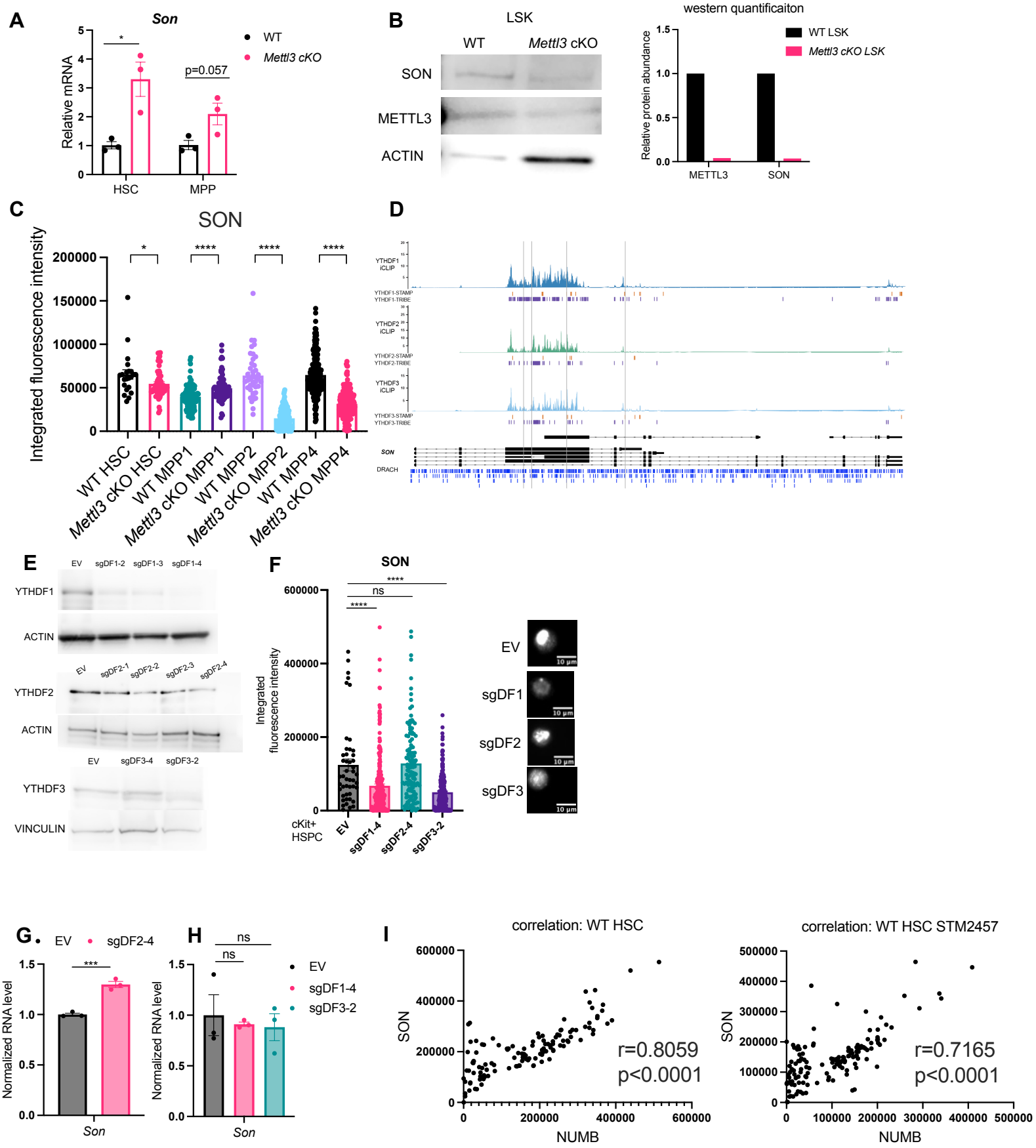
A
Son
Relative mRNA
WT
Mettl3 cKO
p=0.057
HSC
MPP
B
LSK
WT
Mettl3 cKO
SON
METTL3
ACTIN
western quantificaiton
Relative protein abundance
WT LSK
Mettl3 cKO LSK
METTL3
SON
C
SON
Integrated fluorescence intensity
WT HSC
Mettl3 cKO HSC
WT MPP1
Mettl3 cKO MPP1
WT MPP2
Mettl3 cKO MPP2
WT MPP4
Mettl3 cKO MPP4
D
YTHDF1 iCLIP
YTHDF1-STAMP
YTHDF1-TRIBE
YTHDF2 iCLIP
YTHDF2-STAMP
YTHDF2-TRIBE
YTHDF3 iCLIP
YTHDF3-STAMP
YTHDF3-TRIBE
SON
DRACH
E
EV
sgDF1-2
sgDF1-3
sgDF1-4
YTHDF1
ACTIN
sgDF2-1
sgDF2-2
sgDF2-3
sgDF2-4
YTHDF2
ACTIN
sgDF3-4
sgDF3-2
YTHDF3
VINCULIN
F
SON
Integrated fluorescence intensity
cKit+ HSPC
EV
sgDF1-4
sgDF2-4
sgDF3-2
sgDF1
sgDF2
sgDF3
10 µm
G.
EV
sgDF2-4
Normalized RNA level
Son
H
EV
sgDF1-4
sgDF3-2
Normalized RNA level
Son
I
correlation: WT HSC
SON
NUMB
r=0.8059
p<0.0001
correlation: WT HSC STM2457
SON
NUMB
r=0.7165
p<0.0001

Supplementary Figure 2: Depletion of m^{6}A reduces SON protein abundance. Related to Figure 2.
(A) *Son* mRNA was increased in *Mettl3* cKO HSCs and MPPs. qPCR was performed in RNA isolated from purified WT and *Mettl3* cKO HSCs and MPPs. n=3 mice.
(B) SON protein abundance was reduced in *Mettl3* cKO LSKs. WT and *Mettl3* cKO LSKs were sorted from a pool of 3 mice. SON protein abundance was measured by western blotting.
(C) SON protein abundance was reduced in *Mettl3* cKO HSCs, MPP2s and MPP4s, except for MPP1s. Quantification of SON protein abundance by immunofluorescence in WT and *Mettl3* cKO HSCs and MPPs.
(D) YTHDF1/2/3 binding patterns to the *SON* transcript using YTHDF1/2/3 iCLIP, STAMP (YTHDF1/2/3-APOBEC1) and TRIBE (YTHDF1/2/3-ADAR) datasets. These data demonstrate direct binding of the three RBPs in SON, with major signal around the exon 3. Importantly, these data also show that the SON m^{6}A site regions detected by our DART-seq data in human CD34+ HSPCs (gray lines) are located at the identified YTHDF1/2/3 binding sites.
(E) Depletion of YTHDF1, YTHDF2, or YTHDF3 protein in WT cKit+ bone marrow cells using sgRNAs. *Rosa*Cas9 WT cKit+ bone marrow cells were transduced with 2-4 sgRNAs against mouse YTHDF1, YTHDF2, or YTHDF3, GFP+ cells were sorted followed by western blotting. The sgRNAs with the best knockout (sgDF1-4, sgDF2-4, sgDF3-2) were selected. n=3 independent experiments.
(F) Depletion of YTHDF1 or YTHDF3, but not YTHDF2, reduced SON protein abundance in WT cKit+ bone marrow cells. *Rosa*Cas9 WT cKit+ HSPCs were transduced with sgRNA against YTHDF1-3 proteins respectively, GFP+ cells were sorted followed by immunofluorescence. n=3 independent experiments. Left, quantification of SON abundance using immunofluorescence. Right, representative images of SON abundance in each condition.
(G) Depletion of YTHDF2 increased *Son* mRNA expression in WT cKit+ bone marrow cells. *Rosa*Cas9 WT cKit+ bone marrow cells were transduced with sgRNA against YTHDF2, GFP+ cells were sorted followed by qPCR. n=2 independent experiments.
(H) Depletion of YTHDF1 or YTHDF3 does not alter *Son* mRNA expression in WT cKit+ bone marrow cells. *Rosa*Cas9 WT cKit+ bone marrow cells were transduced with sgRNA against YTHDF1 or YTHDF3, GFP+ cells were sorted followed by qPCR. n=3 independent experiments.
(I) SON protein abundance highly correlate with NUMB protein in the paired daughter cell assays. Data in (A), (C), (E), (F), (G) represent means ± s.e.m. , * represents $p < 0.05$. ** represents $p < 0.01$. *** represents $p < 0.001$. **** represents $p<0.0001$. ns represents $p > 0.05$.

Figure S3

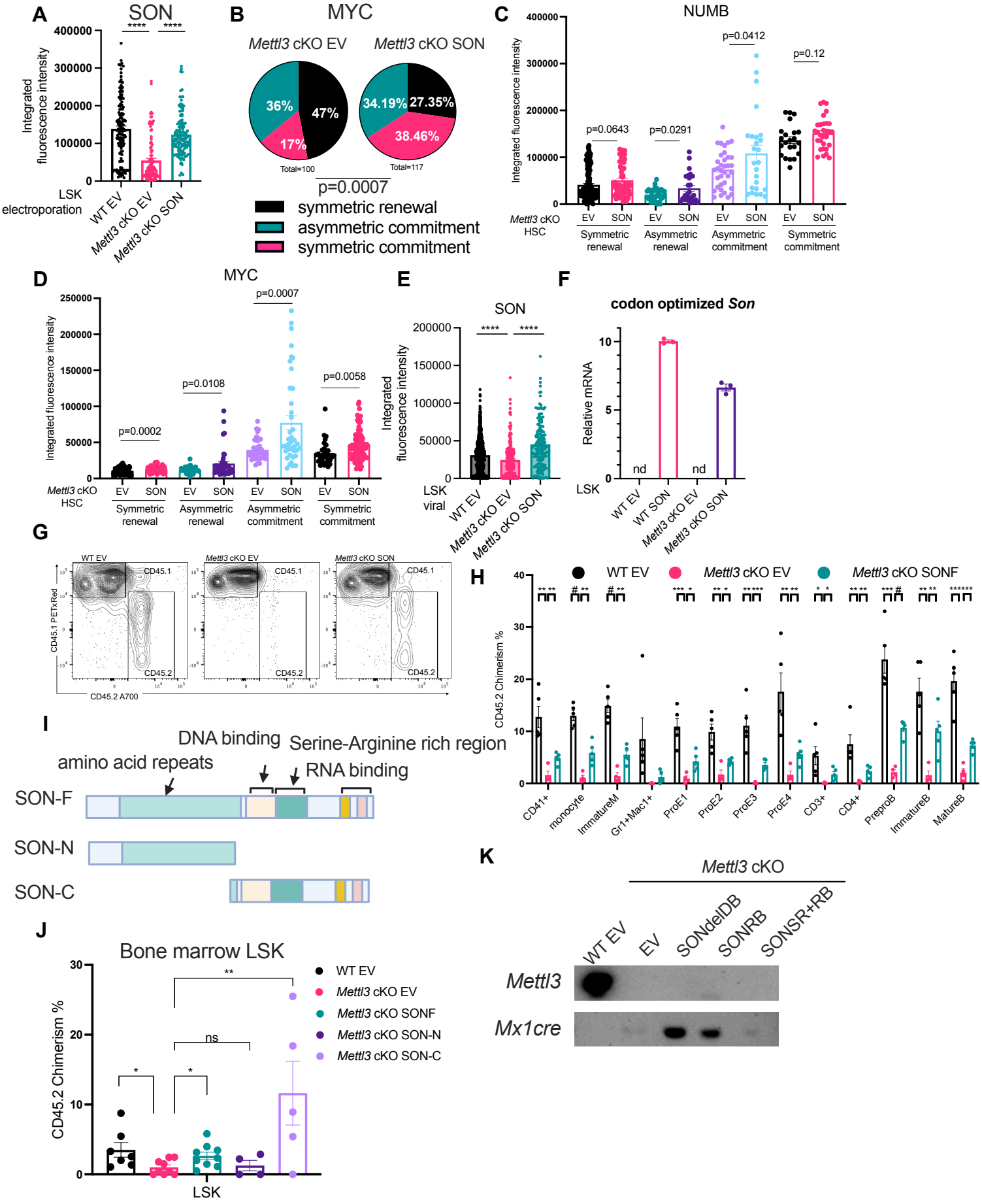
A
SON
Integrated fluorescence intensity
LSK electroporation
WT EV
Mettl3 cKO EV
Mettl3 cKO SON
B
MYC
Mettl3 cKO EV
Mettl3 cKO SON
36%
47%
17%
34.19%
27.35%
38.46%
Total=100
Total=117
p=0.0007
symmetric renewal
asymmetric commitment
symmetric commitment
C
NUMB
Integrated fluorescence intensity
p=0.0643
p=0.0291
p=0.0412
p=0.12
Mettl3 cKO HSC
EV
SON
Symmetric renewal
Asymmetric renewal
Asymmetric commitment
Symmetric commitment
D
MYC
Integrated fluorescence intensity
p=0.0002
p=0.0108
p=0.0007
p=0.0058
Mettl3 cKO HSC
Symmetric renewal
Asymmetric renewal
Asymmetric commitment
Symmetric commitment
E
SON
Integrated fluorescence intensity
LSK viral
WT EV
Mettl3 cKO EV
Mettl3 cKO SON
F
codon optimized Son
Relative mRNA
nd
LSK
WT EV
WT SON
Mettl3 cKO EV
Mettl3 cKO SON
G
WT EV
Mettl3 cKO EV
Mettl3 cKO SON
CD45.1
CD45.2
CD45.1 PETxRed
CD45.2 A700
H
WT EV
Mettl3 cKO EV
Mettl3 cKO SONF
CD45.2 Chimerism %
CD41+
monocyte
ImmatureM
Gr1+Mac1+
ProE1
ProE2
ProE3
ProE4
CD3+
CD4+
PreproB
ImmatureB
MatureB
I
DNA binding
amino acid repeats
Serine-Arginine rich region
RNA binding
SON-F
SON-N
SON-C
J
Bone marrow LSK
CD45.2 Chimerism %
WT EV
Mettl3 cKO EV
Mettl3 cKO SONF
Mettl3 cKO SON-N
Mettl3 cKO SON-C
ns
LSK
K
Mettl3 cKO
WT EV
EV
SONdelDB
SONRB
SONSR+RB
Mettl3
Mx1cre

Supplementary Figure 3: SON rescues the symmetric commitment defect in m^{6}A deficient HSCs. Related to Figure 3.

(A) Increase of SON protein abundance in *Mettl3* cKO LSKs electroporated with SON overexpressing plasmid measured by immunofluorescence.
(B) SON overexpression in *Mettl3* cKO HSC rescues its symmetric commitment defect measured by MYC symmetric high divisions. *Mettl3* cKO HSCs were sorted from a pool of at least 3 mice and electroporated with empty vector or SON overexpressing plasmid. Paired daughter cell assay was then performed using these cells. Percentages of doublet cells in each type of cell division were shown. n=100 (*Mettl3* cKO EV using MYC IF), n=117 (*Mettl3* cKO SON using MYC IF); P value was calculated using Chi-square test.
(C) NUMB abundance was not increased in SON overexpressing cells that underwent a symmetric commitment fate. NUMB protein abundance was measured in each HSC divisions (symmetric renewal divisions (NUMB/MYC low), asymmetric divisions (including NUMB/MYC low and NUMB/MYC high), and symmetric commitment divisions (NUMB/MYC high)) using immunofluorescence.
(D) MYC protein abundance was significantly increased in all HSC fate categories. MYC protein abundance was measured in each HSC divisions (symmetric renewal divisions (NUMB/MYC low), asymmetric divisions (including NUMB/MYC low and NUMB/MYC high), and symmetric commitment divisions (NUMB/MYC high)) using immunofluorescence.
(E) Increase of SON protein abundance in *Mettl3* cKO LSKs transduced with SON overexpressing lentivirus measured by immunofluorescence.
(F) Increase of codon optimized *Son* transcript in WT and *Mettl3* cKO LSKs transduced with SON overexpressing lentivirus measured by qPCR.
(G) Representative flow cytometry plots showing donor engraftment gating in experiments performed in Figure 3E.
(H) SON overexpression rescues the multilineage engraftment of *Mettl3* cKO LSKs. Quantification of the frequency of donor-derived cells in myeloid, erythroid, megakaryocytic, and lymphoid lineages were shown in the peripheral blood at 4-week post transplantation, n = 4-5. n represents number of mice.
(I) Scheme of SON N-terminal and C-terminal truncation mutants. Human *SON* mRNA coding sequence was divided into half, N-terminal, and C-terminal parts.
(J) C-terminal of SON, but not the N-terminal was able to rescue the functional defect of *Mettl3* cKO LSKs. Quantification of the frequency of donor-derived cells was shown in the bone marrow LSK population 9 weeks post transplantation. n=4-9, n represents number of mice.
(K) Genotyping of engrafted donor cells confirms that Mettl3 remains deleted. Engrafted donor cells were sorted, and their genomic DNA were extracted. Genotyping PCR using primers that detects the *Mettl3* exon 4 (the exon that should be excised due to cre activation) and the *Mx1 cre* locus were performed. Data in (A), (C), (D), (E), (F), (H), (J) represent means ± s.e.m. , * represents $p < 0.05$. ** represents $p < 0.01$. *** represents $p < 0.001$. # represents $p<0.0001$. ns represents $p > 0.05$.

Figure S4

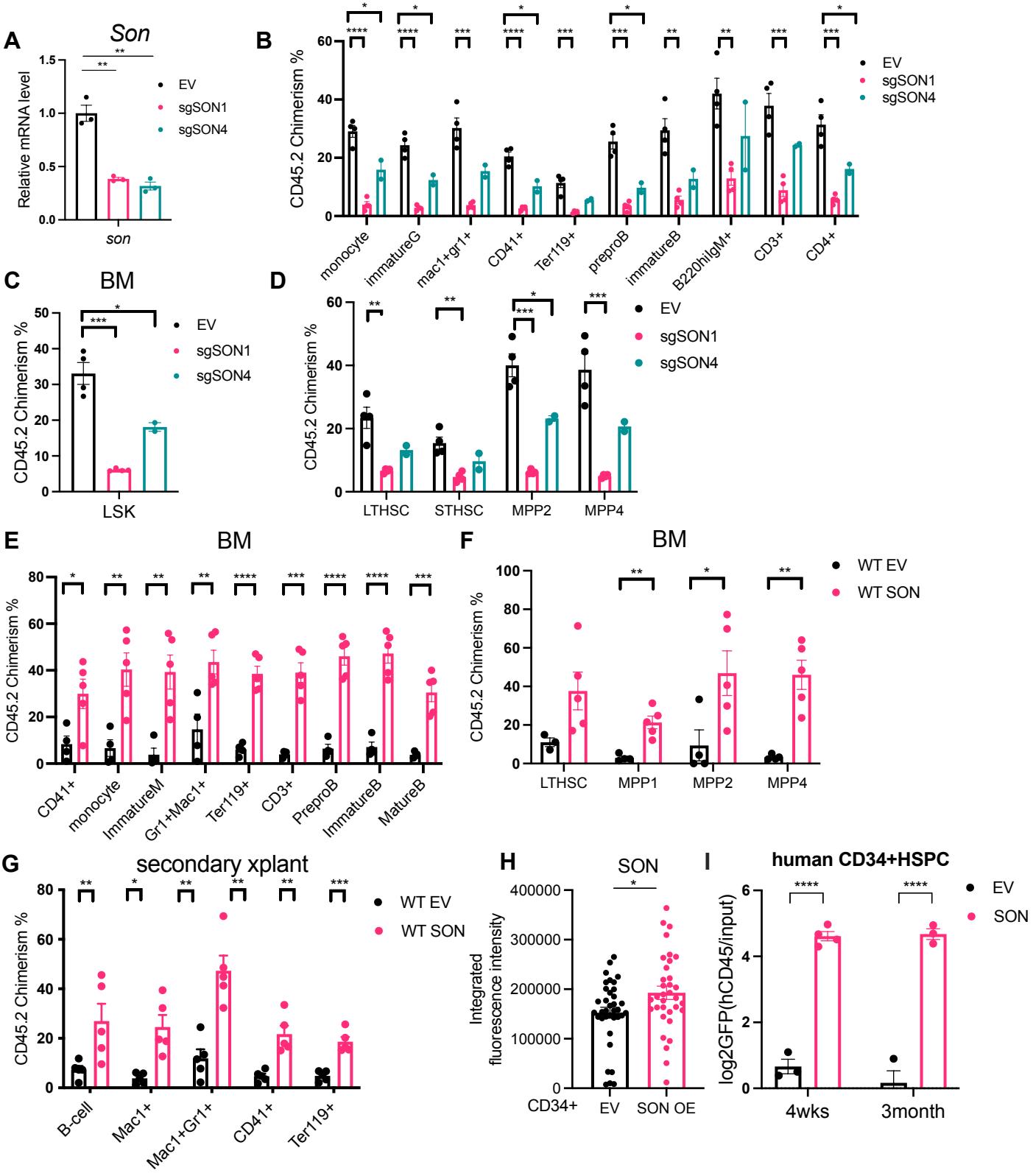
A
Son
Relative mRNA level
son
EV
sgSON1
sgSON4
B
CD45.2 Chimerism %
monocyte
immatureG
mac1+gr1+
CD41+
Ter119+
preproB
immatureB
B220hilgM+
CD3+
CD4+
C
BM
CD45.2 Chimerism %
LSK
D
CD45.2 Chimerism %
LTHSC
STHSC
MPP2
MPP4
E
BM
CD45.2 Chimerism %
CD41+
monocyte
ImmatureM
Gr1+Mac1+
Ter119+
CD3+
PreproB
ImmatureB
MatureB
WT EV
WT SON
F
BM
CD45.2 Chimerism %
LTHSC
MPP1
MPP2
MPP4
G
secondary xplant
CD45.2 Chimerism %
B-cell
Mac1+
Mac1+Gr1+
CD41+
Ter119+
H
SON
Integrated fluorescence intensity
CD34+
EV
SON OE
I
human CD34+HSPC
log2GFP(hCD45/input)
4wks
3month

Supplemental Figure 4: SON is an important hematopoietic stem cell regulator. Related to Figure 4.
(A) *Son* mRNA levels were reduced in the *Rosa*Cas9 LSK cells transduced with sgRNAs against SON measured by qPCR.
(B) Knockdown of SON reduced donor CD45.2 chimerism in the myeloid, erythroid, megakaryocytic, and lymphoid lineages population 5 months post transplantation with sgSON1 and sgSON4 groups. n=2-5, n represents number of mice. Representative of two independent experiments.
(C) Knockdown of SON reduced donor CD45.2 chimerism in LSK population 5 months post transplantation with sgSON1 and sgSON4 groups. n=2-5, n represents number of mice. Representative of two independent experiments.
(D) Knockdown of SON reduced donor CD45.2 chimerism in stem cell populations 5 months post transplantation with sgSON1 and sgSON4 groups. n=2-5, n represents number of mice. Representative of two independent experiments.
(E) SON overexpression in WT LSKs resulted in increased multilineage engraftment in the peripheral blood 4 months post transplantation. n=4-5, n represents number of mice.
(F) SON overexpression in WT LSKs resulted in increased stem cell engraftment 4 months post transplantation. n=4-5, n represents number of mice.
(G) SON overexpression in WT LSKs resulted in increased stem cell engraftment 4 months post transplantation in secondary transplantation. n=5, n represents number of mice.
(H) Increase of SON protein abundance in CD34+ cells transduced with SON overexpressing lentivirus measured by immunofluorescence.
(I) SON overexpression increases in vivo repopulating capacity in human CD34+ cells. Figure S5I are results from an independent repeat of experiment in Figure 5H-I. Human CD34+ cells were purified from at least 6 mixed CB units (each unit from one healthy donor), transduced with empty vector or SON overexpressing lentivirus. Before transplantation, GFP frequency were measured in the input donor cells. 20k transduced human CD34+ cells were then transplanted into NSGS recipient mice and donor engraftment were measured at 4 weeks and 12 weeks post transplantation. GFP frequency in the hCD45 engrafted population were measured and the relative enrichment of GFP+ donor cells were plotted. n=3-4, n represents number of mice. Representative of three independent experiments. Data in (A-I) represent means ± s.e.m. , * represents $p < 0.05$. ** represents $p < 0.01$. *** represents $p < 0.001$. **** represents $p<0.0001$. ns represents $p > 0.05$.

Figure S5

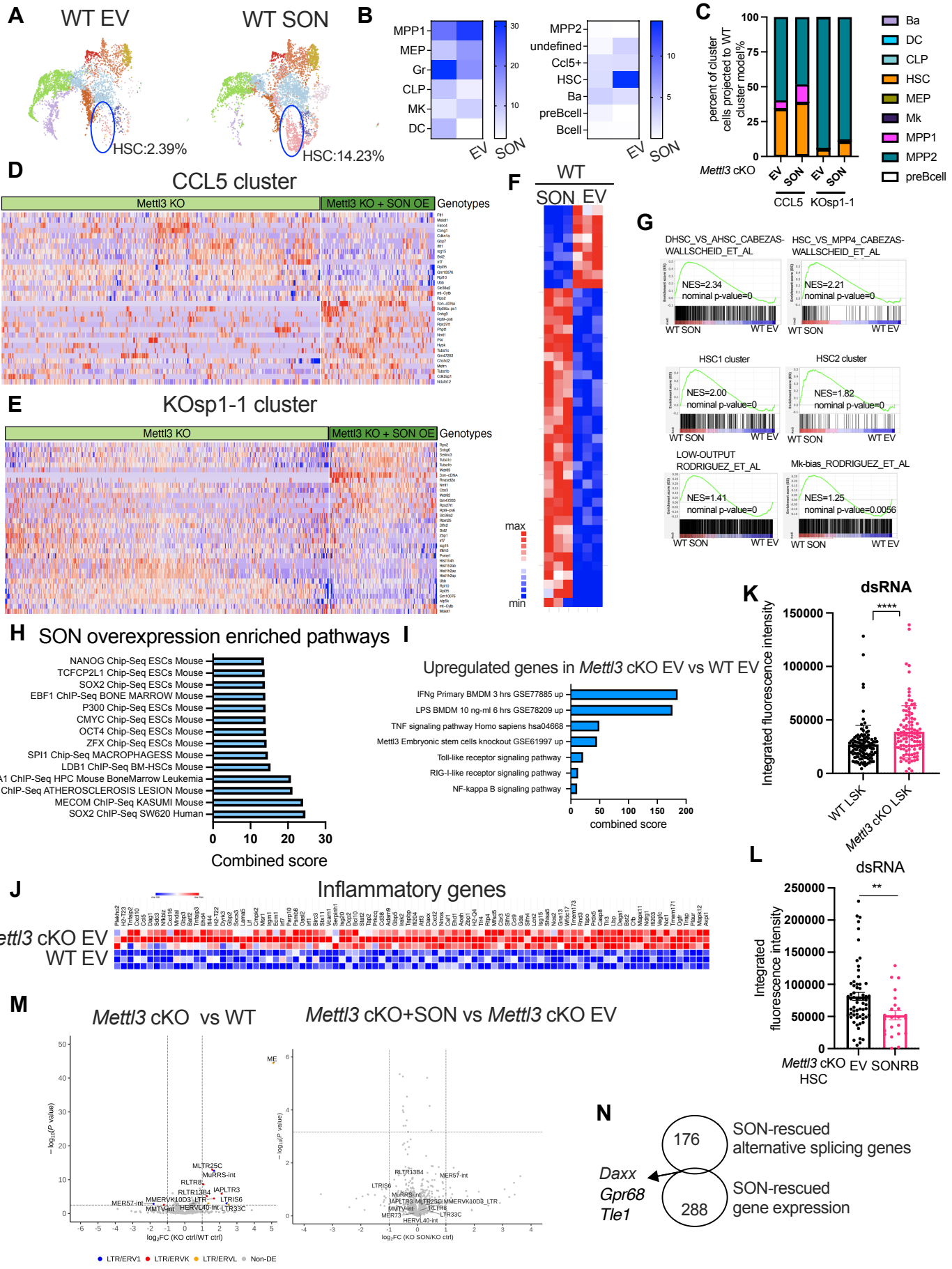
A
WT EV
WT SON
HSC:2.39%
HSC:14.23%
B
MPP1
MEP
Gr
CLP
MK
DC
MPP2
undefined
Ccl5+
HSC
Ba
preBcell
Bcell
EV
SON
C
percent of cluster cells projected to WT cluster model%
Mettl3 cKO
CCL5
KOsp1-1
Ba
DC
CLP
HSC
MEP
Mk
MPP1
MPP2
preBcell
D
CCL5 cluster
Mettl3 KO
Mettl3 KO + SON OE
Genotypes
E
KOsp1-1 cluster
F
WT
SON EV
max
min
G
DHSC_VS_AHSC_CABEZAS-WALLSCHEID_ET_AL
NES=2.34
nominal p-value=0
HSC_VS_MPP4_CABEZAS-WALLSCHEID_ET_AL
NES=2.21
nominal p-value=0
HSC1 cluster
NES=2.00
nominal p-value=0
HSC2 cluster
NES=1.82
nominal p-value=0
LOW-OUTPUT RODRIGUEZ_ET_AL
NES=1.41
nominal p-value=0
Mk-bias_RODRIGUEZ_ET_AL
NES=1.25
nominal p-value=0.0056
WT SON
WT EV
H
SON overexpression enriched pathways
NANOG Chip-Seq ESCs Mouse
TCFCP2L1 Chip-Seq ESCs Mouse
SOX2 Chip-Seq ESCs Mouse
EBF1 ChIP-Seq BONE MARROW Mouse
P300 Chip-Seq ESCs Mouse
CMYC Chip-Seq ESCs Mouse
OCT4 Chip-Seq ESCs Mouse
ZFX Chip-Seq ESCs Mouse
SPI1 Chip-Seq MACROPHAGESS Mouse
LDB1 ChIP-Seq BM-HSCs Mouse
GATA1 ChIP-Seq HPC Mouse BoneMarrow Leukemia
KLF4 ChIP-Seq ATHEROSCLEROSIS LESION Mouse
MECOM ChIP-Seq KASUMI Mouse
SOX2 ChIP-Seq SW620 Human
Combined score
I
Upregulated genes in Mettl3 cKO EV vs WT EV
IFNg Primary BMDM 3 hrs GSE77885 up
LPS BMDM 10 ng-ml 6 hrs GSE78209 up
TNF signaling pathway Homo sapiens hsa04668
Mettl3 Embryonic stem cells knockout GSE61997 up
Toll-like receptor signaling pathway
RIG-I-like receptor signaling pathway
NF-kappa B signaling pathway
combined score
K
dsRNA
****
Integrated fluorescence intensity
WT LSK
Mettl3 cKO LSK
L
dsRNA
**
Integrated fluorescence intensity
Mettl3 cKO HSC
EV
SONRB
J
Inflammatory genes
Mettl3 cKO
EV
WT EV
M
Mettl3 cKO vs WT
Mettl3 cKO+SON vs Mettl3 cKO EV
log2FC (KO ctrl/WT ctrl)
log2FC (KO SON/KO ctrl)
LTR/ERV1
LTR/ERVK
LTR/ERVL
Non-DE
N
176
SON-rescued alternative splicing genes
Daxx
Gpr68
Tle1
288
SON-rescued gene expression

Supplementary Figure 5: SON partially rescues the inflammatory program in *Mettl3* cKO HSCs. Related to Figure 5.

(A) UMAP of WT empty vector and WT SON overexpressing LSKs from single-cell RNA sequencing (scRNA-seq) showed an expansion of the HSC cluster.
(B) Quantification of cell frequencies of different clusters in WT EV, WT SON LSK cells based on scRNA-seq.
(C) Increased projection to WT HSC cluster with SON overexpression in both CCL5 and KOsp1-1 clusters. Maximum likelihood of the CCL5 and KOsp1-1 cluster in *Mettl3* cKO EV and *Mettl3* cKO SON overexpressing samples into the WT EV expression models was performed based on the transcriptome profile from scRNA-seq.
(D) Differential gene expression analysis between *Mettl3* cKO EV and *Mettl3* cKO SON overexpressing CCL5 cluster. The default Wilcox-Rank sum test in FindMarkers was used to identify differential expressed genes present in at least 25% of the cells in either group (min.pct = 0.25). The final set of DEGs (differential expressed genes) was determined by filtering for a P value adjusted < 0.05.
(E) Differential gene expression analysis between *Mettl3* cKO ctrl and *Mettl3* cKO SON overexpressing KOsp1-1 cluster. The default Wilcox-Rank sum test in FindMarkers was used to identify differential expressed genes present in at least 25% of the cells in either group (min.pct = 0.25). The final set of DEGs was determined by filtering for a P value adjusted < 0.05.
(F) Heatmap showing the differential expressed genes between the WT EV and WT SON overexpressing LSK cells. (cut-off for the differential expressed genes: padj <0.1)
(G) GSEA analysis showing the pathways enriched in the WT SON overexpressing cells using the gene expression rank-list comparing WT EV vs WT SON in LSKs.
(H) Enrichr pathway enrichment analysis of the genes that were upregulated expressed between WT ctrl and WT SON. (cut-off for the differential expressed genes: padj <0.1)
(I) Enrichr pathway enrichment analysis of the genes that were differentially expressed between WT EV and *Mettl3* cKO EV LSKs. (cut-off for the differentially expressed genes: padj < 0.05)
(J) Heatmap showing the upregulation of inflammatory genes in *Mettl3* cKO EV LSKs compared to WT EV.
(K) Increased dsRNA amount in *Mettl3* cKO LSKs. Quantification of dsRNA abundance by immunofluorescence in each group. n=2 independent experiments.
(L) SON-RB reduces the dsRNA amount in *Mettl3* cKO LSKs. Quantification of dsRNA abundance by immunofluorescence in each group.
(M) SON overexpression does not rescue the altered endogenous retrovirus expression in *Mettl3* cKO LSKs. Volcano plot showing log2-transformed fold change (log2FC) in retrotransposon expression in *Mettl3* cKO EV versus WT EV LSKs (left) and *Mettl3* cKO SON versus *Mettl3* cKO EV LSKs (right) using random assignment of multi-mapped reads. Blue, red, and orange denote significantly deregulated RepeatMasker annotations belonging to ERV1, ERVK, and ERVL, respectively. Grey denotes non-differentially expressed (non-DE) retrotransposons. P values were computed using DESeq2 and adjusted with the Benjamin–Hochberg Procedure (Methods). abs(log2FC) >= 1; false discovery rate (FDR) <= 0.05.
(N) Only three genes overlap between the SON-rescued alternative splicing gene targets and SON-rescued differential expressed genes.

Figure S6

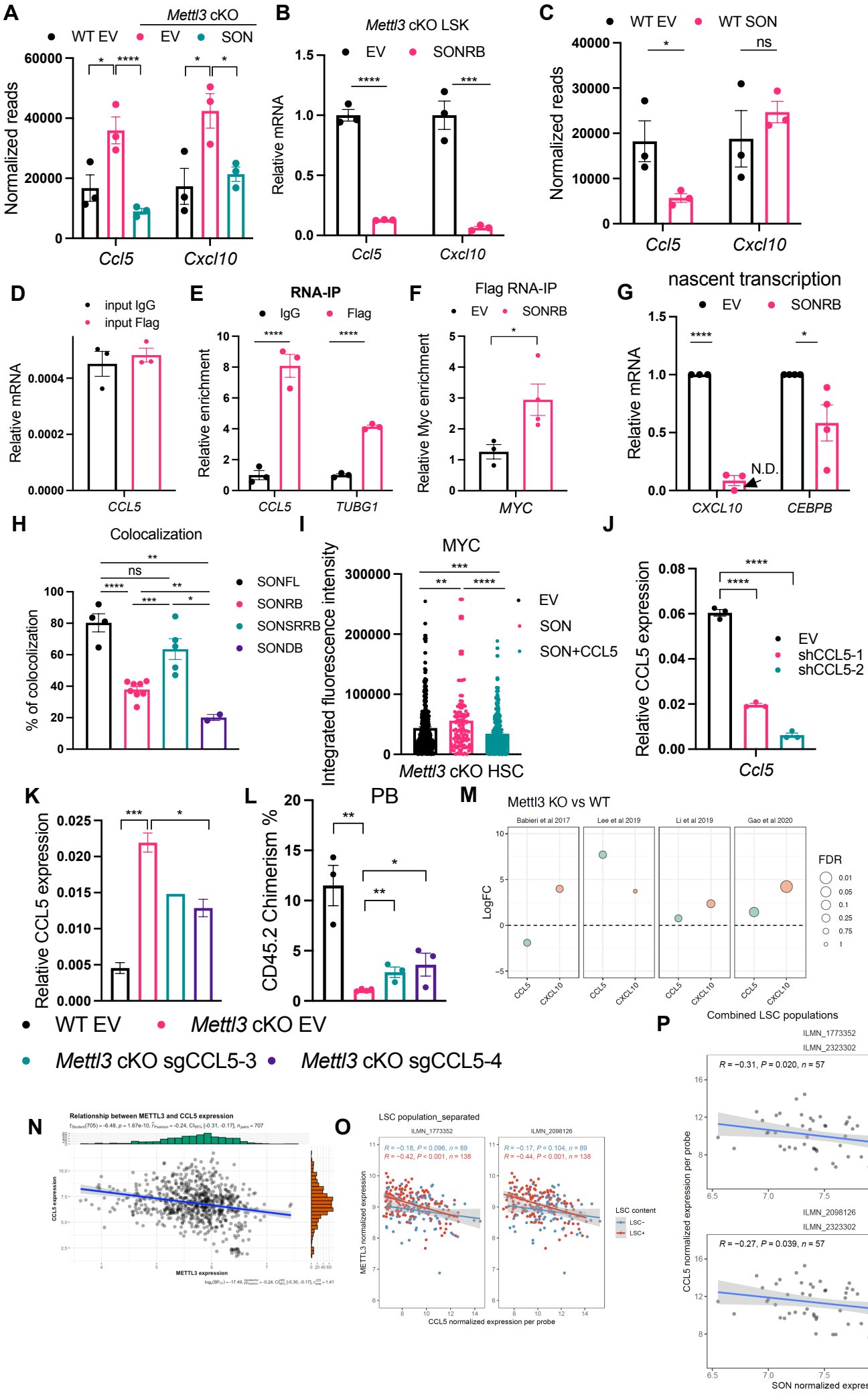
A
Mettl3 cKO
WT EV
EV
SON
Normalized reads
Ccl5
Cxcl10
B
Mettl3 cKO LSK
EV
SONRB
Relative mRNA
C
WT EV
WT SON
ns
Normalized reads
D
input IgG
input Flag
Relative mRNA
CCL5
E
RNA-IP
IgG
Flag
Relative enrichment
TUBG1
F
Flag RNA-IP
Relative Myc enrichment
MYC
G
nascent transcription
N.D.
CXCL10
CEBPB
H
Colocalization
% of colocolization
SONFL
SONRB
SONSRRB
SONDB
I
MYC
Integrated fluorescence intensity
Mettl3 cKO HSC
SON+CCL5
J
Relative CCL5 expression
shCCL5-1
shCCL5-2
K
L
PB
CD45.2 Chimerism %
M
Mettl3 KO vs WT
Babieri et al 2017
Lee et al 2019
Li et al 2019
Gao et al 2020
LogFC
FDR
Combined LSC populations
WT EV
Mettl3 cKO EV
Mettl3 cKO sgCCL5-3
Mettl3 cKO sgCCL5-4
N
Relationship between METTL3 and CCL5 expression
METTL3 expression
O
LSC population_separated
ILMN_1773352
ILMN_2098126
METTL3 normalized expression
CCL5 normalized expression per probe
LSC content
P
ILMN_1773352
ILMN_2323302
ILMN_2098126
CCL5 normalized expression per probe
SON normalized expression

Supplementary Figure 6: CCL5 is a downstream of SON that controls HSC symmetric commitment fate. Related to Figure 6.

(A) Both Ccl5 and Cxcl10 transcripts were rescued by SON overexpression in *Mettl3* cKO LSKs. Normalized RNA-seq read counts of *Ccl5* and *Cxcl10* transcripts in WT EV LSK, *Mettl3* cKO EV and *Mettl3* cKO SON overexpressing LSKs. n=3 independent assays.
(B) SON-RB reduces *Ccl5* and *Cxcl10* expression in *Mettl3* cKO LSKs. Quantifications of *Ccl5* and *Cxcl10* expression in *Mettl3* cKO LSKs with EV, SON-RB overexpression using qPCR. n=3 independent assays.
(C) *Ccl5*, but not *Cxcl10*, was downregulated by SON overexpression in WT LSKs. Normalized RNA-seq read counts of *Ccl5* and *Cxcl10* transcripts in WT EV LSK and WT SON overexpressing LSKs. n=3 independent assays.
(D) CCL5 expression levels remain comparable in SON-RB overexpressing THP1 cells input samples used for IgG or Flag RNA IP.
(E) SON-RB binds to the CCL5 transcript in THP1 cells. RNA-IP in THP1 cells expressing SON-RB-Flag retrovirus using mouse IgG antibody or Flag antibody followed by RNA extraction and qPCR of target genes. n=3, n represents independent experiments.
(F) SON-RB binds to MYC transcript in THP1 cells. RNA-IP in THP1 cells expressing empty vector (MIG) or SON-RB-Flag retrovirus followed by qPCR targeting MYC transcript. n=3 independent assays.
(G) SON-RB suppresses nascent transcription of the CXCL10 and CEBPB transcripts in THP1 cells. n=3 independent experiments.
(H) SON-RB colocalizes to endogenous nuclear speckles. 293T cells were transfected with Flag tagged fragments include SON-FL (full length), SON-RB, SON SR+RB, or SON DB. Colocalization of Flag and endogenous SON were measured based on confocal images using Fiji.
(I) Upregulation of MYC abundance were blocked with CCL5 treatment in *Mettl3* cKO LSK with SON overexpression. Quantifications of MYC protein abundance in *Mettl3* cKO LSKs with EV, SON overexpression with or without CCL5 treatment using immunofluorescence.
(J) Knockdown of *Ccl5* mRNA levels using shRNAs against *Ccl5* in the *Mettl3* cKO LSK cells measured by qPCR. n=3 independent assays.
(K) Knockdown of *Ccl5* mRNA levels using sgRNAs against *Ccl5* in the *Rosa*CAS9 *Mettl3* cKO LSK cells measured by qPCR. n=3 independent assays.
(L) Depletion of CCL5 in *Mettl3* cKO LSKs using sgRNAs improves engraftment capacity. Quantification of the frequency of donor-derived cells was shown in the peripheral blood 4 weeks post transplantation. n=3-4, n represents number of mice. Data in (A-L) represent means ± s.e.m. , * represents $p < 0.05$. ** represents $p < 0.01$. *** represents $p < 0.001$. **** represents $p<0.0001$. ns represents $p > 0.05$.
(M) Reported Log fold changes in expression of CCL5 and CXCL10 genes across Mettl3 cKO or METTL3 KO versus WT RNA-seq datasets in mouse and human. False discovery rate values are indicated with the corresponding circle size, with more significant values having a bigger area.
(N) Scatter plot showing a negative correlation between METTL3 and CCL5 expression in BEAT-AML patient datasets (n = 707).
(O) The negative correlation of METTL3 and CCL5 expression is more significant in leukemia stem cell positive patients compared to the leukemia stem cell negative patient samples (138 LSC+ and 89 LSC-) of an AML cohort GSE76009 (n = 78). CCL5 is measured by two probes, consequently the associated expression is separated by probe.
(P) Negative correlation between SON and CCL5 in METTL3 low expressing patients (the 25% lowest percentile) in the same dataset as (N). In both top and bottome panels, x axis represents SON normalized expression, and y axis represents CCL5 normalized expression for two different probes detecting CCL5 (top ILMN_1773352; bottom ILMN_2098126).